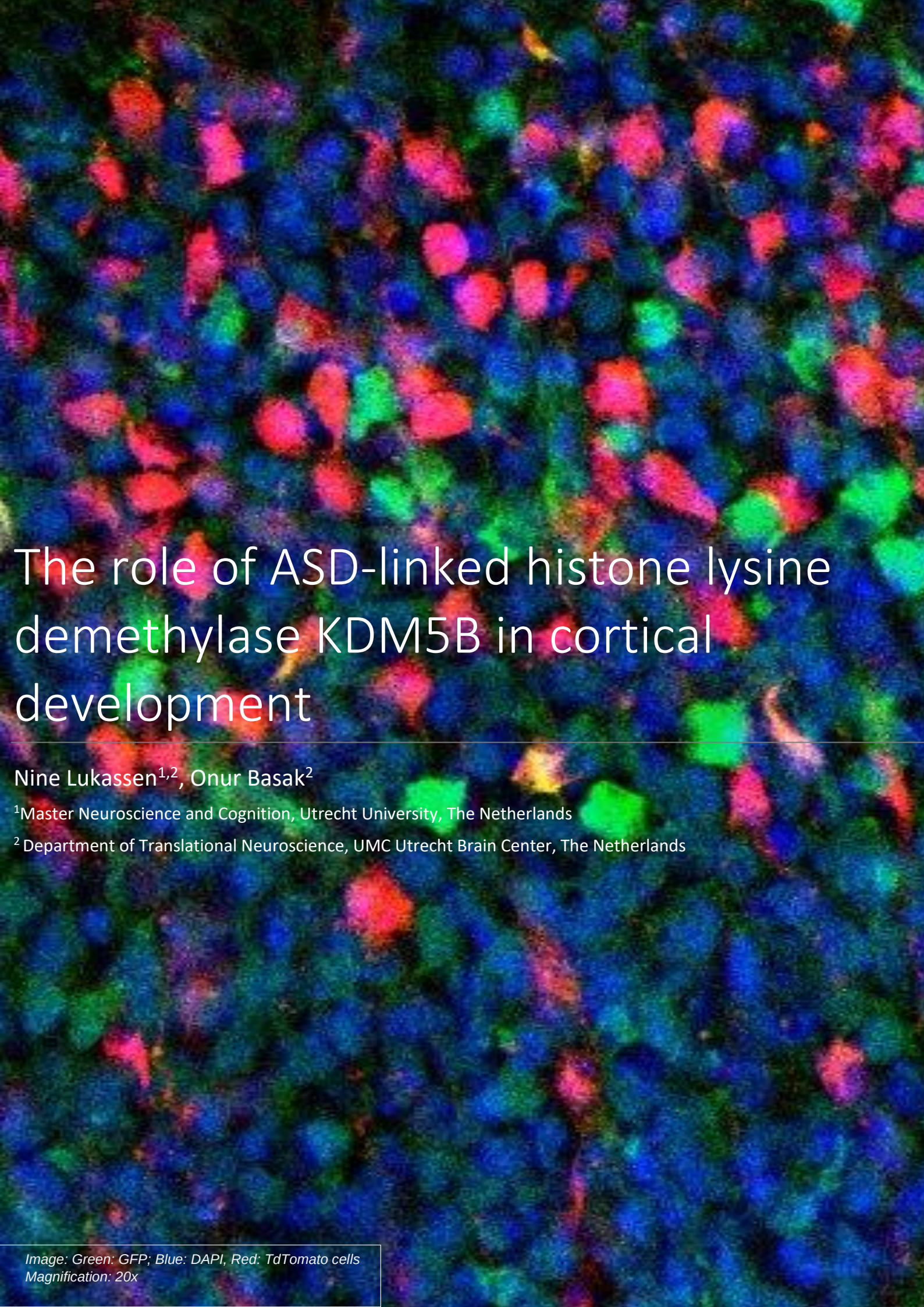

The role of ASD-linked histone lysine demethylase KDM5B in cortical development

Nine Lukassen[1,2], Onur Basak[2]

[1]Master Neuroscience and Cognition, Utrecht University, The Netherlands

[2] Department of Translational Neuroscience, UMC Utrecht Brain Center, The Netherlands

Image: Green: GFP; Blue: DAPI, Red: TdTomato cells
Magnification: 20x

Acknowledgement

This report summarizes the project I did for my major internship of nine months, and that time went by quickly. For this, I have to thank all the members of the Basak lab. First of all, and most importantly, Onur Basak for being my supervisor during my internship. Despite his busy schedule, he always had time for our weekly meetings, in which he patiently explained the theory behind all the steps of the project. He let me come up with my own plan, or at least guided me in the right direction. I also want to thank Tiziana Hey. I could always count on her to help me out. She often recognized what I was struggling with and gave me advice on how to fix it, or how to do certain things differently in the future. I learnt a lot from her on how to be a better researcher.

Of course, I was not the only master student at the Department of Translational Neuroscience. First, I want to thank the other students in the Basaklab: Alexandra de Reus, Bram Schouten and Tarik Boulahlib. Alexandra for always offering her support and our lovely chats in the student room, Bram for always being critical during our lab meetings and thereby improving my presentations and Tarik for reminding me of how much I have learnt during my internship. Second, Solée Pop, the master student who worked on this project before me. Her detailed previous work made it easier for me to pick up where she left off.

Lastly, I want to thank Youri Adolfs and Nicky van Kronenburg for performing the *in utero* electroporation with me and always helping me with all the other questions I had. Roland van Dijk, Keith Garner and Ilia Timpanaro for performing the FACS for me. All the members of the Hollab for letting me join their meetings, journal clubs and lab outings, and thereby also teaching me a lot about Alzheimer's Disease and microglia.

Abstract

Epigenetic mechanisms are of great importance in the temporal and spatial regulation of the formation of the cortex. Disruption can result in neurodevelopmental disorders, such as autism spectrum disorder (ASD). Multiple mutations in the human KDM5B gene, which is a histone demethylase that removes histon-3-lysin-4 (H3K4) methyl modifications, have been linked to ASD. KDM5B and H3K4me3 have been associated with both differentiation of NSCs and self-renewal of NSCs. A KDM5B KO has been generated before to study the effect of KDM5B, but the role of KDM5B in late embryonic and early postnatal development, as well as the downstream targets and mechanisms of KDM5B, remains poorly understood.

The aim of this project is to investigate the function of KDM5B in cortical development, which I will do by generating a KDM5B KO with a CRISPR/Cas9 pipeline that was optimised in the Basak Lab. To disrupt the function of KDM5B, I designed, amplified and cloned four different gRNAs that are part of a pCAG-Cre-U6-4xgRNA construct. Next, I introduced plasmids containing this construct in NSCs with an *in utero* electroporation (IUE) at embryonic day 13 (E13) and isolated the embryos at E17. To validate the efficiency of the CRISPR/Cas9 complex, I analysed the loss of GFP fluorescence in the control group during FACS. Immunohistochemistry shows a lower expression of KDM5B in the mutant, indicating the successful generation of a KDM5B KO. This KDM5B KO results in a relatively lower number of cells below cortical layers V and VI. A lower percentage of KDM5B KO cells among the live cells during FACS suggests a possible indispensable effect of KDM5B on the proliferation of NSCs. This is supported by the observation that KDM5B is highly expressed in the ventricular zone. By generating a KDM5B KO, I thus show that KDM5B potentially is involved in the proliferation of NSCs. These are the first steps in determining the function of KDM5B in corticogenesis, which can help in unravelling how bivalent chromatin modifications affect the development of the cortex, and how this might be altered in ASD patients. This will contribute to our overall understanding of the role of epigenetic regulation in ASD.

Layman's Summary

Autism spectrum disorder (ASD) is caused by a disturbed brain development. It is characterized by deficits in social interaction and communication, repetitive behaviours and impaired intelligence development. An estimated 1% of the population worldwide is affected by ASD. The fact that monozygotic twins, who share 100% of their DNA, are often both affected by ASD suggests that ASD is heritable. A lot of research has been done trying to find mutations in the DNA that are involved in the development of ASD. One mutated gene that is often linked to ASD is histone lysine demethylase 5B (KDM5B). KDM5B can change the structure around the DNA, which will result in less synthesis of the protein encoded by that particular gene. This is called epigenetic regulation. KDM5B is just one protein in a whole system of epigenetic regulators that regulate the development of the cortex. It is suggested that these different epigenetic regulators interact with each other.

To discover the role of KDM5B in cortical development, I wanted to disrupt the functioning of KDM5B. CRISPR/Cas9 is a system that can create small breaks in the KDM5B gene, which will disturb the functioning of the KDM5B protein. This is called a KDM5B knock-out (KO). A few days after the Kdm5b gene is destroyed in mouse embryos, I looked at the effect of this KDM5B KO on the development of the cortex. It showed that there are fewer cells below the cortex. This can be due to a smaller increase in cell numbers, which is called proliferation. Stem cells are the only cells in the brain that can proliferate. KDM5B appears to be particularly important for these stem cells. During my internship, I was thus not only able to generate a KDM5B KO, but I also identified the importance of KDM5B during the proliferation of stem cells in the cortex. Without KDM5B, it is possible that these stem cells die or become a different cell type that does not proliferate.

My project is one of the first steps in figuring out how the epigenetic regulator KDM5B is involved in the development of the cortex. This can help in exploring the role of this whole system of epigenetic regulators in cortical development in future studies. Determination of the involvement of this system in the development of the cortex will help explore the potential role of altered epigenetic regulation in ASD patients.

Introduction

The cerebral cortex and more particularly the neocortex is responsible for higher cognitive and motor functions. It consists of six layers, which are all formed during the embryonic development of the cortex. The formation of these layers depends on temporally and spatially regulated molecular and cellular signals, which are partially regulated by epigenetic regulation (Lodato & Arlotta, 2015; Lui et al., 2011; Mukhtar & Taylor, 2018).

At the start of the development of the cortex, the neocortex only exists of two adjacent sheets. The ventricular zone (VZ) contains the neural stem cells (NSCs) and is covered by the preplate (PP) (Gesuita & Karayannis, 2021; Mukhtar & Taylor, 2018). NSCs can divide and will form the neural progenitor cells that eventually produce all the different types of neurons found in the cortex. First, the NSCs undergo symmetric divisions to expand the neural progenitor pool because this symmetrical division results in two identical neural progenitors (Mukhtar & Taylor, 2018; Stiles & Jernigan, 2010). After this expansion phase, there is a shift from symmetrical to asymmetrical cell division, which marks the start of neurogenesis (E10.5-E18.5 in mice) (Fig. 1). A division now leads to one new NSC and one neural progenitor, which will start to migrate towards the preplate (Gesuita & Karayannis, 2021; Stiles & Jernigan, 2010).

The first neurons to be formed and start migration form the marginal zone (MZ) that will later become layer I. In contrast to neural progenitors of layer I that can migrate by themselves, neurons that form the other cortical layers cannot cover the required distance by themselves (Genescu & Garel, 2021; Gesuita & Karayannis, 2021; Götz & Huttner, 2005; Mukhtar & Taylor, 2018; Woodworth et al., 2012). To continue neurogenesis and migration, the neural progenitor cells turn into radial glial cells (RGCs) that stay connected to the VZ. RGCs will be used by many new neurons to migrate towards their respective layer in the embryonic cortex (Fig. 1) (Genescu & Garel, 2021; Gesuita & Karayannis, 2021; Mukhtar & Taylor, 2018; Stiles & Jernigan, 2010). Despite their name suggesting that RGCs are glial cells, they are still NSCs that contribute to neurogenesis. Basal progenitors (BPs) are derived from NSCs. BPs will form the subventricular zone (SVZ), which is a mitotic region located basally of the VZ. BPs undergo several symmetric cell divisions that result in two neuronal daughter cells during each division. The dividing BPs in the SVZ will be the primary source of cortical neurons during neurogenesis in mice (Götz & Huttner, 2005; Mukhtar & Taylor, 2018).

The neurons that are formed migrate along the RGCs. The first neurons that arrive will form cortical layer VI, which is the deepest layer of the cortex. The rest of the layers will be formed in an inside-out manner. In mice, layer VI is formed around E12.5, layer V at E13.5 and layer IV at E14.5. Layer II and III will be formed last at E15.5 (Fig. 1). Differentiation of the newly generated neurons makes sure that all six layers contain different neuron cell types that project to different brain regions (Mukhtar & Taylor, 2018; Woodworth et al., 2012). When

almost all cortical layers are formed at E17.5, NSCs begin to generate astrocytes and ependymal cells, which continues postnatally (Mukhtar & Taylor, 2018; Yao & Jin, 2014). While most NSCs have migrated to the cortex, some NSCs remain in the SVZ. These NSCs no longer proliferate but can start dividing again during adult neurogenesis (Götz & Huttner, 2005; Yao & Jin, 2014).

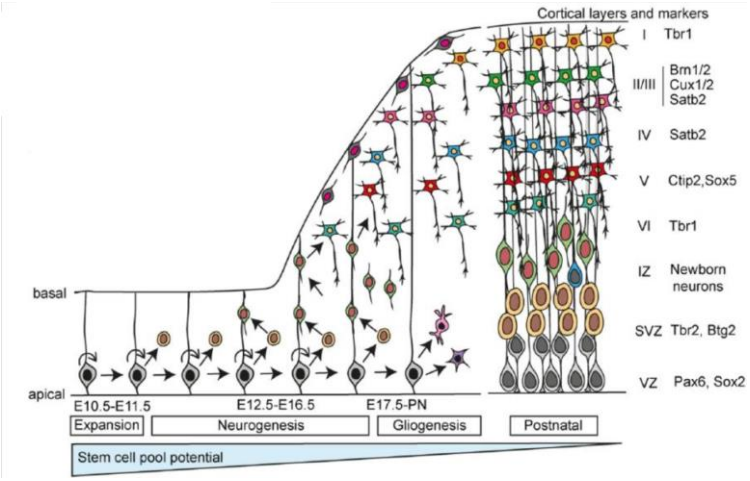

Figure 1 Formation of the six cortical layers during embryonic and early postnatal development. *After an expansion phase that ends at E11.5, neurogenesis starts. NSCs start migrating towards their cortical layer and continue differentiating. Meanwhile, the stem cell pool potential is reduced. The six layers are formed in an inside–out fashion. Neurogenesis ends at E17.5, which is when gliogenesis starts. Both the migration of neurons and gliogenesis will continue postnatally (Mukhtar & Taylor, 2018).*

The formation of the six cortical layers with their different neuronal subtypes is a process that is tightly regulated. Epigenetic mechanisms are of great importance in this temporal and spatial regulation of cell fate choice (Yao et al., 2016). Epigenetics is often described as the heritable changes in gene expression and chromatin structure that are not the result of alterations in DNA sequence, and include DNA methylation, histone modification and non-coding RNAs (Salinas et al., 2020; Yao et al., 2016; Yoon et al., 2020). These modifications control the accessibility of DNA and histones and thereby control gene activation and silencing. In this way, epigenetic mechanisms influence the expression of key regulators that in turn regulate the proliferation and differentiation of NSCs (Salinas et al., 2020; Yao et al., 2016). It is crucial for cortical development that these epigenetic mechanisms work correctly. Disruptions of epigenetic regulation have been implicated in multiple brain diseases. Mutations in regulators of histone modification have been regularly connected to neurodevelopmental diseases, such as autism spectrum disorder (ASD) (Ronan et al., 2013; Salinas et al., 2020; Yoon et al., 2020).

ASD is a very heterogeneous neurodevelopmental disorder, but it can be characterized by deficits in social interaction and communication, repetitive behaviours and varying levels of impaired intelligence development (Garcia-Forn et al., 2020; Lord et al., 2020; Yoon et al.,

2020). As of 2015, it is estimated that 1% of the general population is affected by ASD (Baxter et al., 2015; Vos et al., 2016). In the United States, one in 54 children is diagnosed with ASD in 2016 (Maenner et al., 2020). Twin studies offered the first compelling evidence for the involvement of genetics in the aetiology of ASD, by showing the heritability of ASD (Gaugler et al., 2014; Masini et al., 2020; Tick et al., 2016). Genome-wide association studies (GWAS) have led to the identification of common variants that are involved in ASD. These common variants consist of single nucleotide polymorphisms (SNPs). Despite their small effect sizes, the additive effect of SNPs can have a substantial impact on ASD liability (Garcia-Forn et al., 2020; Gaugler et al., 2014; Masini et al., 2020)

However, common variation cannot fully explain the aetiology of ASD. Techniques such as whole-exome sequencing (WES) helped identify rare *de novo* mutations implicated in ASD. *De novo* mutations include copy number variations (CNV) and single nucleotide variations (SNVs) or indels. CNVs can influence gene expression, whereas SNVs and indels can result in *de novo* loss-of-function mutations (De Rubeis et al., 2014; Garcia-Forn et al., 2020; Masini et al., 2020). With WES studies, Satterstrom *et al. (2020)* were able to identify 102 ASD-associated genes. While *de novo* mutations have a large effect on the individual, they hardly explain the overall pathology. The interplay between common variants and rare *de novo* mutations is suggested to result in the heterogeneous manifestations of ASD (De Rubeis et al., 2014; Grove et al., 2019; Masini et al., 2020).

Several WES studies have identified KDM5B as a high confidence ASD gene (Chen et al., 2017; De Rubeis et al., 2014; Sanders et al., 2015; Satterstrom et al., 2020). KDM5B is part of the histone lysine demethylase (KDM) family and is responsible for the demethylation of lysine 4 of histone H3 (H3K4) (Fig. 2). KDM5B has also been implicated in multiple cancers, in particular in breast cancer (Xhabija & Kidder, 2019). The trimethylation of H3K4 (H3K4me3) can predominantly be found at transcription start sites and has been linked to active transcription (Barski et al., 2007; Mosammaparast & Shi, 2010; Pokholok et al., 2005). The presence of H3K4me3 facilitates transcription by changing the chromatin structure (De Dieuleveult et al., 2016) and forming a binding site for certain transcription factors (Lauberth et al., 2013; Van Ingen et al., 2008; Vermeulen et al., 2007). Promoters in embryonic stem cells (ESCs) indeed show a high level of H3K4me3, but this does not immediately result in the active transcription of these genes. Many H3K4me3 positive promoters are also marked by H3K27me3, which in turn represses gene expression (Albert et al., 2017). This bivalent chromatin modification can be found in many cell types, but it is relatively high in ESCs and NSCs where it marks developmental and lineage genes. Bivalency is thought to ensure that all lineage options remain open during embryonic development (Albert & Huttner, 2018; Bernstein et al., 2006). With this in mind, it is proposed that neuronal genes receive both the

active H3K4me3 and repressive H3K27me3 mark when ESCs differentiate into NSCs and that the presence of this bivalent mark ensures that these neuronal genes are repressed but primed to be expressed during future neuronal differentiation (Harikumar & Meshorer, 2015; Schmitz et al., 2011; Yao et al., 2016).

Ezh2 is the histone lysine methyltransferase that is responsible for generating H3K27me3. Ezh2 is part of the polycomb repressive complex (PRC2) together with SUZ12 and EED (Fig. 2). Deletion of Ezh2 has a negative effect on the repression of neuronal genes and thereby disrupts differentiation of neuronal progenitors (Corley & Kroll, 2015; Pereira et al., 2010; Zhang et al., 2014). Two SNPs of Ezh2 have been linked to ASD (Li et al., 2016).

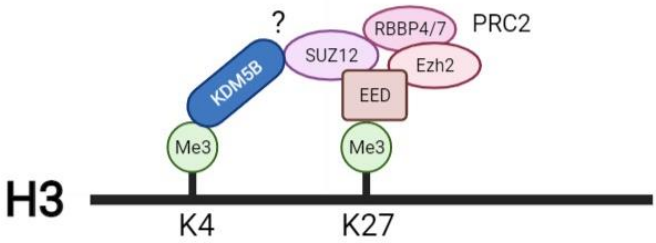

Figure 2 KDM5B binds to H3K4me3 and interacts with PRC2. *KDM5B binds to H3K4me3 but is also able to interact with PRC2 by binding to SUZ12. PRC2 binds to H3K4me27, where Ezh2 is responsible for the methylation of H3K27. Bivalent chromatin modification is established by the presence of both H3K4me3 and H3K27me3.*

In vitro studies show that KDM5B is not required for the self-renewal of ESCs. If ESCs are depleted of KDM5B, they appear to be unable to switch off specific stem cell genes during differentiation. This suggests that KDM5B is necessary for initiating the differentiation of NSCs (Kidder et al., 2014; Schmitz et al., 2011). However, other studies propose that KDM5B is actually required for the proliferation of ESCs and suppress differentiation during this (Cederquist et al., 2020; Dey et al., 2008). Interestingly, KDM5B is thought to cooperate with PRC2 by interacting with SUZ12 (Fig. 2). Within this interaction, KDM5B acts as a co-activator of retinoic acid instead of as a repressor (Zhang et al., 2014). Other studies have also shown KDM5B to be associated with active gene transcription (Kurup et al., 2019; Xie et al., 2011) The role of KDM5B in corticogenesis, therefore, remains to be elucidated.

The aim of this study is to look at the role of KDM5B during mouse cortical development using a combination of genome editing mediated gene inactivation and *in utero* electroporation (IUE). The generation of a conditional knock-out (KO) mouse line is not possible in our study, since previous studies have shown that the breeding of a conditional germline is time-consuming (Albert et al., 2013; Kalebic et al., 2016). Furthermore, generating a KO by deleting the target gene is often lethal during development or the plasticity of the brain might end in compensation of the deleted gene (Albert et al., 2013; Kalebic et al., 2016; Shinmyo et al., 2016; Straub et al., 2014). A pipeline to inactivate genes involving CRISPR/Cas9 has been developed in the

Basak Lab, which was first used to look at the role of Ezh2 on late embryonic and early postnatal cortical development. CRISPR/Cas9 refers to clustered regularly interspaced short palindromic repeats (CRISPR) and CRISPR associated protein 9 (Cas9). Cas9 is an endonuclease that is targeted by a guide RNA (gRNA) towards a specific DNA target, where it will create a double-strand break (Adli, 2018; Doudna & Charpentier, 2014; Hsu et al., 2014). The cell tries to repair this double-strand break by non-homologous end-joining (NHEJ). The error-prone NHEJ results in random insertions or deletions (indels) of nucleotides. These indels often generate a frameshift mutation that can disrupt the function of the targeted protein (Adli, 2018; Hsu et al., 2014; Kalebic et al., 2016).

To achieve our goal, we inactivated KDM5B with a plasmid containing four gRNAs and pCAG-Cre. Inactivated KDM5B will be referred to as a KDM5B KO. We introduced this construct in the cortex at E13 with an IUE The embryos possess the RosaCas9/LSL-TdTomato alleles. Electroporation of the targeted cells results in the expression of Cre recombinase that will fuse the LoxP sites and thereby remove the stopcodon. Consequently, TdTomato is only expressed in the electroporated cells. At E17, I isolated the electroporated brains. I then validated the inactivation of KDM5B with both FACS analysis and immunohistochemistry. After this validation of the KDM5B KO, we investigated the possible effect on cortical development. With immunohistochemistry, I studied the role of KDM5B in migration. Studying the localization of TdTomato+ cells relative to layers V and VI shows a lower number of TdTomato+ cells below layers V and VI in the KDM5B KO. Analysis of FACS data shows a lower relative number of TdTomato+ cells in the mutant, which indicates disruption of the proliferation of KDM5B KO cells. We also investigated the expression levels of KDM5B during cortical development in wildtype mice, which showed us that KDM5B is predominantly expressed in the VZ at E17. We thus show that KDM5B is particularly important for neurogenesis in the VZ and newborn neurons.

Results

KDM5B expression increases during embryonic and early postnatal development of the cerebral cortex

To better understand the possible effect of a KDM5B KO, we studied the expression of KDM5B during embryonic and early postnatal development of the cerebral cortex. Immunohistochemistry of the cortex at different timepoints during embryonic and postnatal development indicated that the relative expression levels of KDM5B change during development (Fig. 3A). KDM5B showed a higher intensity on E13, E18 and P4, whereas the expression level appears lowest on E10 and E17. To further explore this pattern, we collected cortices in triplicate at the same timepoints used for immunohistochemistry with the addition of

the adult cortex. Primers were designed to target the exons of KDM5B to amplify the KDM5B mRNA present (Table IV). Next, we analysed cDNA generated from the isolated cortex in triplicate with RT-qPCR. GAPDH and β-actin were used to normalize the expression levels when calculating the relative fold gene expression level ($2^{-\Delta\Delta Ct}$). The relative expression level of KDM5B at E17 (3,78 ± 0,96) and P4 (2,72 ± 0,48) was significantly higher than E10 (1,38 ± 0,58, p = 0,029; p = 0,040), E13 (1,01 ± 0,54, p = 0,020, p = 0,015), P7 (1,22 ± 0,26, p = 0,036, p = 0,017) and adult (0,53 ± 0,35, p = 0,018, p = 0,004) (Fig. 3B). The higher relative expression level of KDM5B on P4 was also reflected by the observation of the higher intensity of the KDM5B staining on P4. While RT-qPCR showed a significantly higher expression level of KDM5B on E17, the intensity of KDM5B staining appeared higher on E18 instead of E17.

Altogether, KDM5B is present in the cerebral cortex during embryonic and early postnatal development at varying levels. There is an increase in relative expression levels of KDM5B around E17 and at P4.

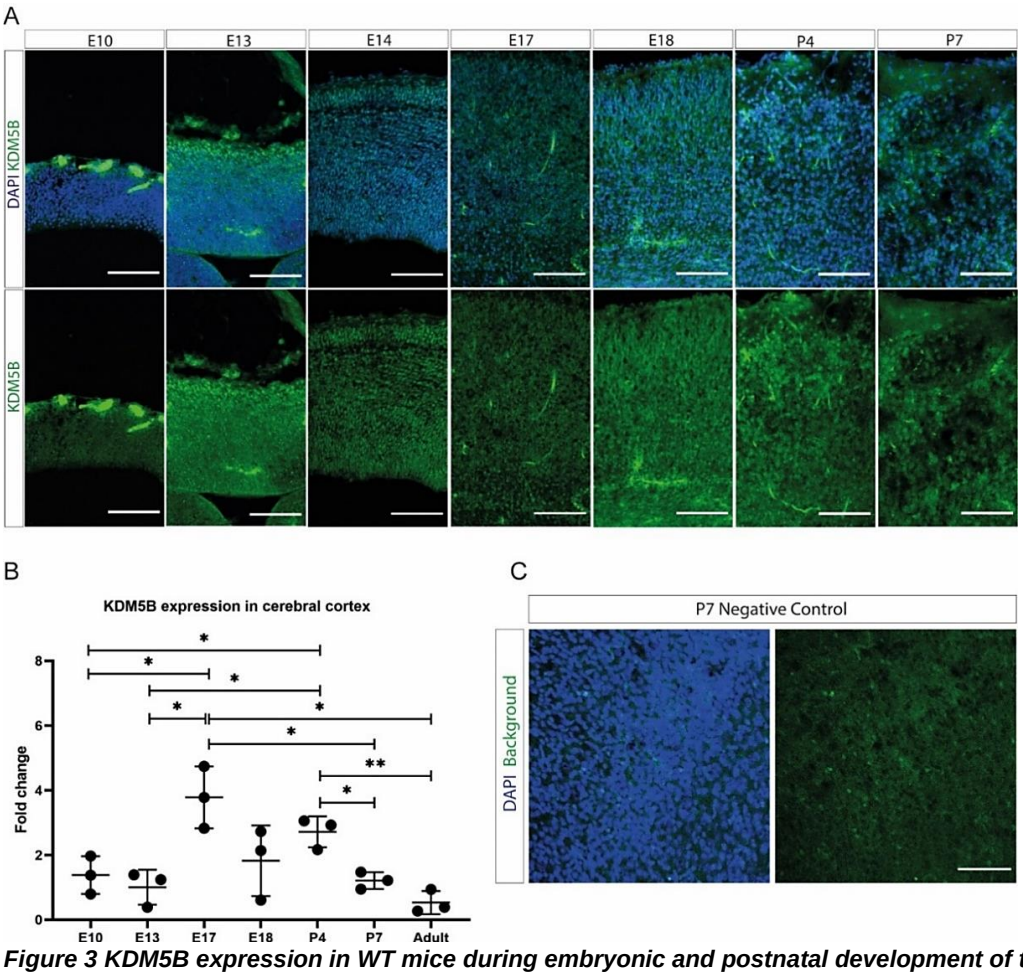

Figure 3 KDM5B expression in WT mice during embryonic and postnatal development of the cortex.

(A) KDM5B protein expression in the cortex seems to fluctuate during cortical development up until the developed cortex, with a higher expression at E13, E18, P4 and P7, and appearing to have a lower expression at E10, E14 and E17. Scale bars = 100 µm. Images taken with a confocal microscope.

*(B) Quantitative PCR shows a significantly higher KDM5B mRNA expression at E17 and P4. Statistics: unpaired, parametric Welch's T-test; N = 3; * = P < 0.05; ** = P < 0.01.*

(C) Negative control. Scale bar = 100 µm.

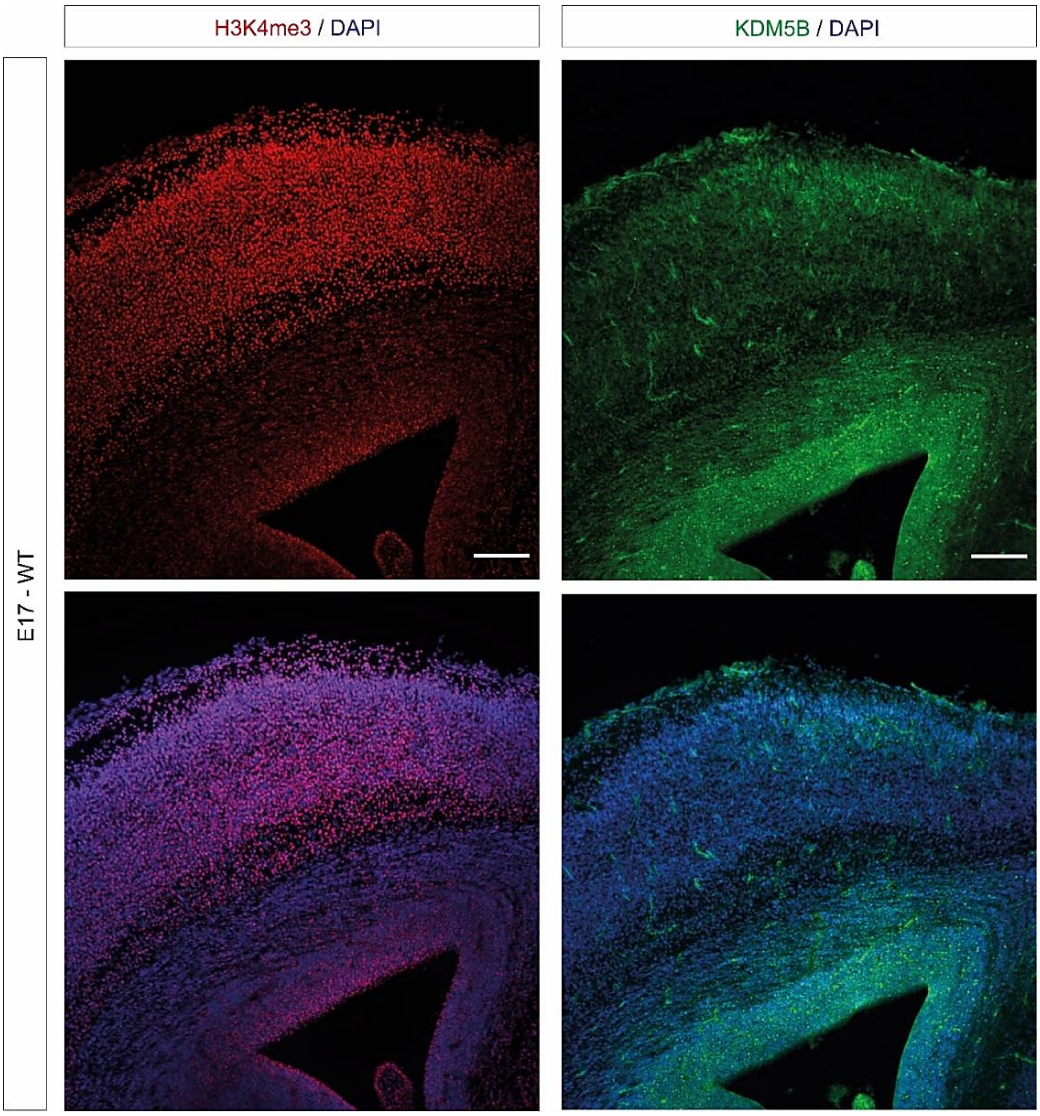

Figure 4 Location of H3K4me3 and KDM5B in the developing cortex at E17*.*

H3K4me3 can mostly be found in cells in the cortex, while KDM5B is highly expressed in the VZ in WT mice at E17. Scale bars = 500 µm. Images taken with an epifluorescence microscope

KDM5B demethylates H3K4me3 in the ventricular zone and less in the cortical layers

KDM5B is responsible for the demethylation of H3K4me3, which marks active transcription. To get a better overview of the presence of H3K4me3 and KDM5B throughout the developing cortex, we did an immunohistochemistry staining for H3K4me3 and KDM5B at E17. While H3K4me3 can predominantly be found in the cortex, KDM5B is mostly localized around the ventricles (Fig 4). There is indeed not much overlap in high intensity between H3K4me3 and KDM5B. These data show us that KDM5B predominantly demethylates H3K4me3 in the VZ and that the H3K4me3 mark is restored after the expression of KDM5B decreases in cells that have reached the cortex.

pCAG-Cre-U6-4xgRNA construct is used to generate a KDM5B KO in mice

To further explore the role of KDM5B in cortical development, we generated a KDM5B KO with the CRISPR/Cas9 system. For CRISPR/Cas9, we designed four gRNAs with a CRISPR gRNA design tool (https://www.benchling.com/crispr/) (Fig 5A). For the gRNAs, we selected sequences of 20 nucleotides followed by a PAM sequence that is essential for the function of Cas9. The on- and off-target scores were considered while selecting a gRNA. The first gRNA targets the transcriptional start site (TSS) to reduce the expression of KDM5B. The other three gRNAs target the functional domains JmjN, PHD1 and PHD3 to disrupt the activity of KDM5B. As a control, we designed four gRNAs that target GFP, so the control group still is subjected to a functional CRISPR/Cas9 system. The gRNAs were amplified and cloned in a pCAG-Cre-U6 construct separately, before being isolated, amplified again and inserted in the same pCAG-Cre-U6 construct with Gibson assembly. We sent this pCAG-Cre-U6-4xgRNA construct for Sanger sequencing to confirm the correct insertion of the gRNAs. No major mutations in the gRNA were observed in the sequencing results (Fig. 5B). Sequencing results for the target site of gRNA2 and the rest of the sequenced fragment were unclear. The two indicated mutations in gRNA2 thus do not certainly confirm a mutation in gRNA2. Therefore, we decided to continue with these constructs. With an IUE, we introduced the pCAG-Cre-U6-4xgRNA construct into heterozygous embryos at E13, to ensure that we target most of the cortical layers. These heterozygous embryos express Cas9 in every neuron under the influence of the ROSA promotor (Fig. 5C). GFP is also expressed under the influence of the same promotor. Expression of TdTomato is repressed by a floxed stopcodon. Delivery of the pCAG-Cre-U6-4xgRNA introduces Cre recombinase in the cells, which will remove the stopcodon and thereby initiate the expression of TdTomato in electroporated cells and their progeny. In this way, we can visualize the targeted region (Fig. 5C-D). Since changes in the growth of the PFC have been linked to ASD and several high confidence ASD-genes have been found to be involved in neurogenesis in the PFC, we decided to target the PFC (Cederquist et al., 2020; Courchesne et al., 2007; Gilbert et al., 2008) Earlier experiments with IUE have tried targeting the PFC, but the results were inconsistent (data not shown). Targeting the motor and somatosensory cortex was more consistent, and since this region is still close to the PFC, we decided to target the motor and somatosensory cortex (Fig. 5D). We thus target the somatosensory and motor cortex during IUE delivery of our pCAG-Cre-U6-4xgRNA plasmid, upon which the electroporated cells will start to express TdTomato+.

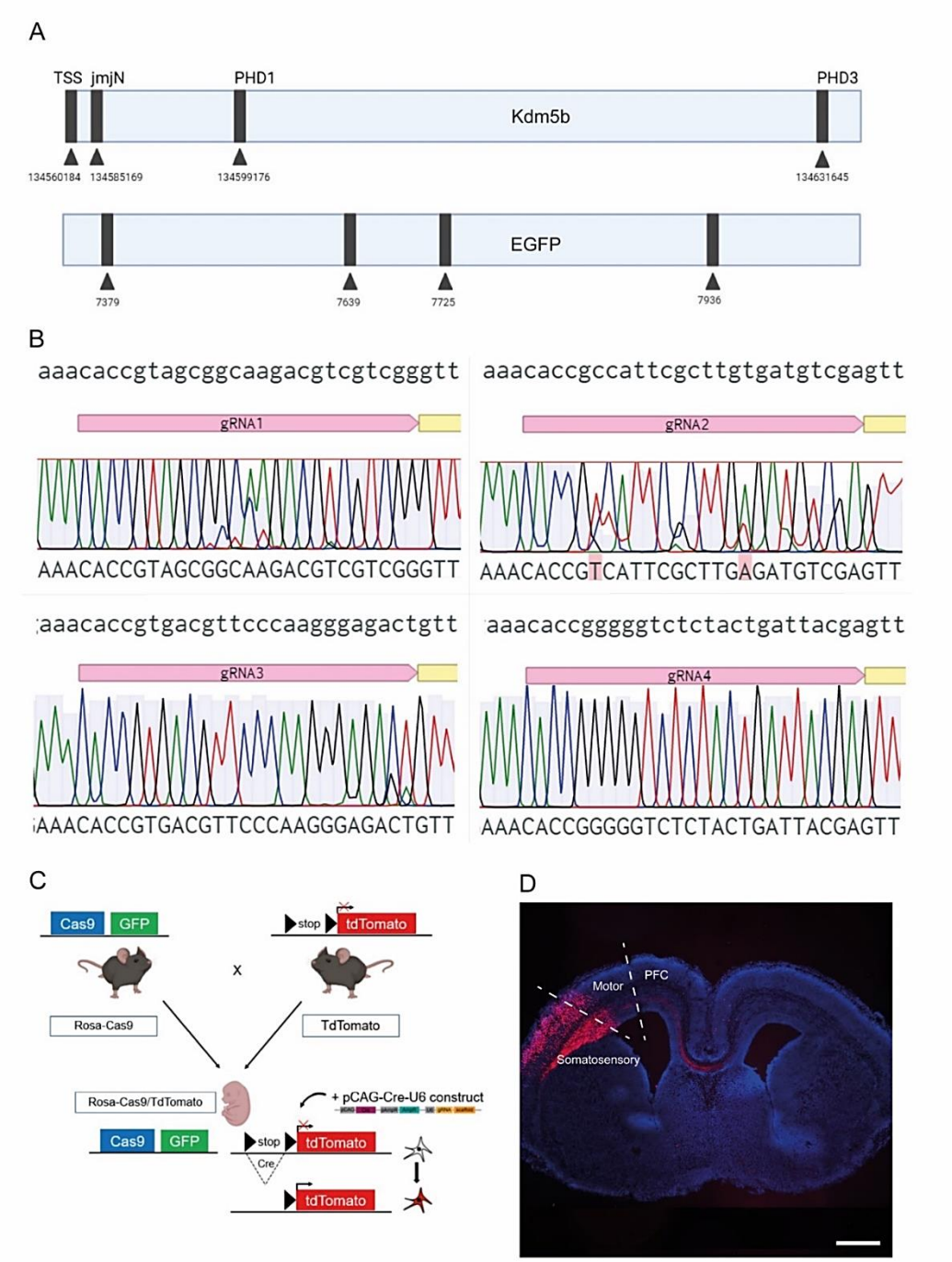

Figure 5 Overview of in utero electroporation to deliver the 4xgRNA construct.

(A) Target sites of the 4 gRNAs included in the pCAG-Cre-U6-4xgRNA construct, indicated by the arrows. gRNAs target the transcriptional start site (TSS) of Kdm5b and the functional domains JmjN, PHD1 and PHD3. A pCAG-Cre-U6-4xgRNA construct targeting EGFP is introduced in the control group, with four different target sites.

(B) Sanger sequencing results of the individual gRNAs. The clear sequencing results of gRNA1, 3 and 4 do not show any mutations. The sequencing results of gRNA2 are less clear, which led to identification of two potential mutations (red box).

(C) Overview of the genetic background of the double heterozygous embryos. Cas9 and GFP are expressed in every cell in the brain under the control of the Rosa promoter. TdTomato is proceeded by a floxed stop codon, which represses its expression. Upon delivery of the pCAG-Cre-U6-4xgRNA construct, Cre binds to the LoxP sites and removes the stop codon, thereby initiating the expression of TdTomato in electroporated cells.

(D) Overview at E17 of the targeted region with the in utero electroporation, where TdTomato+ cells are the electroporated cells. Most cells are located in the somatosensory cortex, but a small part of the motor cortex is also hit. Scale bar = 500 µm.

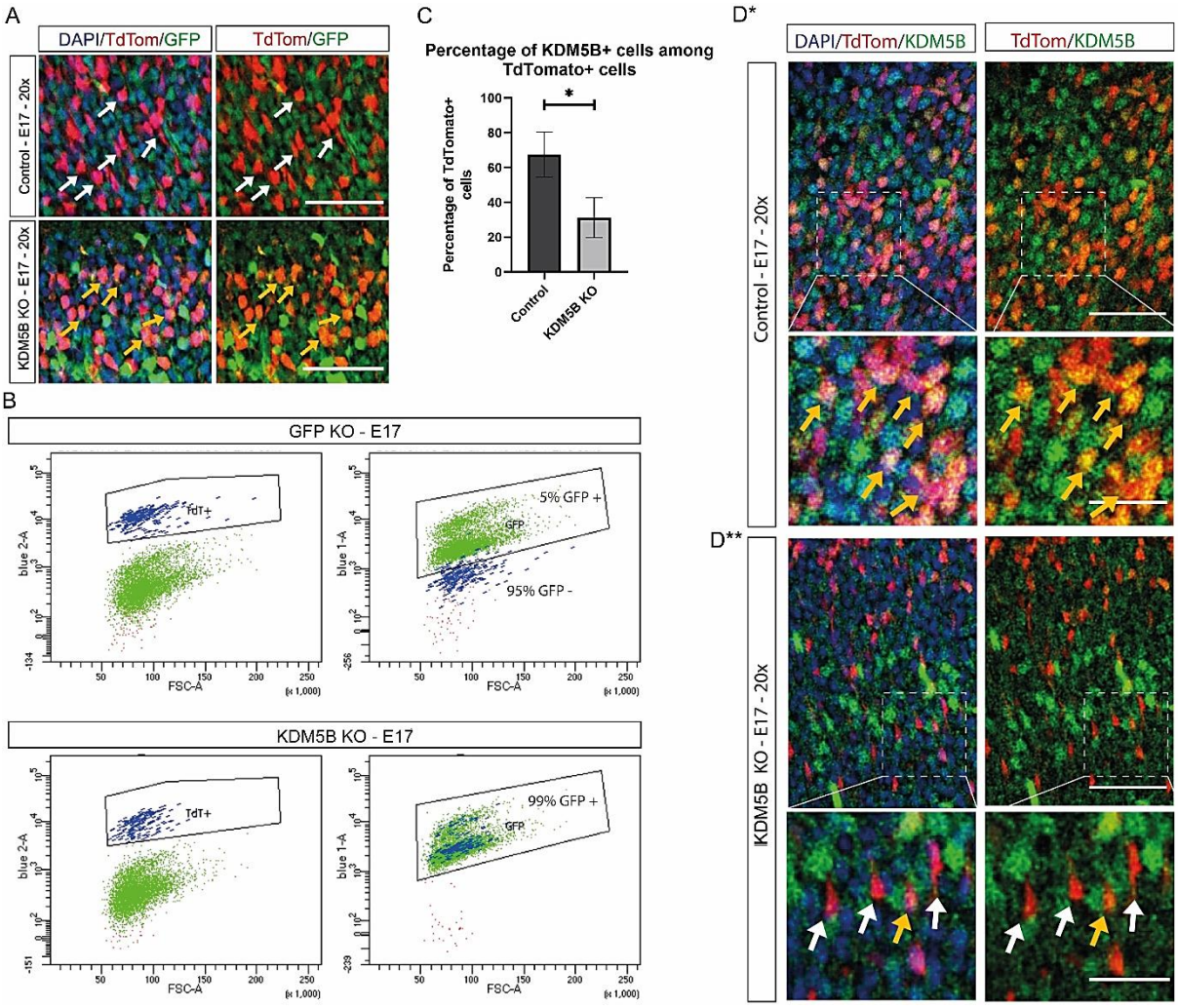

Figure 6 The pCAG-Cre-U6-4xgRNA and CRISPR/Cas9 is efficient to create a KDM5B KO.

(A) Microscopic images of the GFP KO control at E17 show no colocalization of TdTomato+ cells with GFP, as indicated by the white arrows. TdTomato+ cells in the KDM5B KO at E17 express GFP, indicated by yellow arrows. Scale bar = 50 µm. Images with confocal microscope.

(B) FACS analysis of GFP KO control and KDM5B KO. 95% of the TdTomato+ cells do not express GFP, validating the efficiency of the CRISPR/Cas9 system. GFP is still expressed in the KDM5B KO.

*(C) Validation of KDM5B KO by looking at colocalization of TdTomato and KDM5B. Expression of KDM5B by TdTomato+ cells is significantly lower in KDM5B KO. Statistics: unpaired, parametric Welch's T-test; Mean ± SD; KDM5B KO, N = 4; GFP KO, N = 3; * = P < 0.05.*

(D) Confirmation of the KDM5B KO on a protein level. (D) TdTomato+ cells in the GFP KO control express KDM5B, indicated with the yellow arrows. (D**) In the KDM5B KO, there is less or no colocalization of TdTomato+ cells with KDM5B, as indicated by the white arrows. Scale bar upper panel = 50 µm, scale bar lower panel = 25 µm. Images with confocal microscope.*

The CRISPR/Cas9 pipeline is sufficient to create a KDM5B KO

After we introduced the pCAG-Cre-U6-4xgRNA construct in embryos at E13, we looked at both the functioning of the CRISPR/Cas9 system and the expression of KDM5B at E17 to validate the successful establishment of the KDM5B KO. CRISPR/Cas9 function is validated by looking at the expression of GFP in TdTomato+ cells in the GFP KO control, where CRISPR/Cas9 targets the GFP gene. Microscopic pictures showed us that in the GFP KO control TdTomato+ cells do not express GFP (white arrows), while there is a clear colocalization of TdTomato+

cells with GFP in the KDM5B KO (yellow arrows) (Fig. 6A). We verified this by registering the percentage of TdTomato+ cells that express GFP during FACS. In the KDM5B KO, 99% of the TdTomato+ cells express GFP. In contrast, only 5% of the TdTomato+ cells express GFP in the GFP KO control (Fig. 6B), indicating that the CRISPR/Cas9 system is functional. Next, immunohistochemistry staining for KDM5B allowed us to look at the expression of KDM5B on a protein level. Quantification of colocalization of the TdTomato+ cells with KDM5B shows that 68% (±13%, n = 3) of the TdTomato+ cells express KDM5B in the control (Fig. 6C). The percentage of TdTomato+ cells that express KDM5B in the KDM5B KO is significantly lower compared to the control (31%, ±11%, n = 4, p = 0,017). In the GFP KO control, there is a clear colocalization of KDM5B and TdTomato+ cells, as indicated by the yellow arrows (Fig. 6D*). Colocalization of TdTomato and KDM5B was less clear in mutant, which is indicated by the white arrows (Fig. 6D**). To further confirm the KDM5B KO, a pipeline involving Sanger sequencing of the TdTomato+ cells isolated during FACS is being established for the four target sites of the gRNAs. In this system, we isolate DNA from the isolated TdTomato+ cells and amplify this. The isolated DNA will be sent for Sanger sequencing with primers we designed to flank the target sites of the four gRNAs. Unfortunately, we could not finish establishing this system during the course of the project.
In brief, so far the CRISPR/Cas9 is shown to be functional after the introduction of pCAG-Cre-U6-4xgRNA, resulting in a reduced expression of KDM5B in the mutant.

KDM5B KO influences the localisation of electroporated TdTomato+ cells.

After the first indication that the creation of the KDM5B KO was successful, we could study the effect of the KDM5B KO. A possible effect on the migration pattern of NSCs was explored by looking at the location of TdTomato+ cells. An immunohistochemistry staining with Ctip2, which is a marker for cortical layer V and VI, was used as a reference (Fig. 7A). The amount of TdTomato+ cells below, in and above layer V and VI was counted manually on sections obtained from brains isolated at E17. First, we attempted an automated counting of TdTomato+ cells using Fiji(ImageJ) (see methods). Automated counting of cells below layer V / VI was inconsistent due to unreliable counting of merged TdTomato+ in the VZ. Therefore we performed manual counting to be able to distinguish individual TdTomato+ cells and get a more reliable result. We decided upon using relative numbers of TdTomato+ cells below, in and above layer V and VI, because the number of electroporated cells and the electroporated area differs between each replicate. Comparison of absolute numbers of cells is therefore not accurate.

Comparison between the mutant and the control revealed that the relative number of TdTomato+ cells below layer V and VI is significantly lower in the KDM5B KO (41% ± 8%, n = 3, p = 0,030; Fig. 7B). A trend of a higher relative number of TdTomato+ cells above layers V

and VI in the KDM5B KO compared to the control was also observed, but this was not statistically significant. To gain a better insight into this localisation pattern, we used DAPI staining on coronal sections from E17 to divide the developing cortex in the VZ and SVZ, intermediate zone (IZ), and layer V / VI and the cortical plate (CP) (Fig. 7C). Although we obtained no statistically significant results, there is a trend of a lower relative number of TdTomato+ cells in the VZ, SVZ (20% ± 4%, n = 4, p = 0,24) and IZ (25% ± 6%, n = 4, p = 0,34) of the mutant compared to the control (Fig. 7D). These results reflect the trend seen in the localization of TdTomato+ cells relative to Ctip2 staining. By using DAPI to divide the cortex, we split the area below layer VI and V into the VZ and SVZ, and the IZ while combining layers V and VI and the area above these layers. Dividing the area below layer V and VI into two different regions can explain the discrepancy in statistically significance between the two quantification methods of the localisation.

Taken together, the relative amount of TdTomato+ cells below layers V and VI in the mutant is lower compared to the control. This implies that KDM5B is important for the localisation of cells below layers V and VI.

KDM5B KO results in a lower number of alive cells during FACS

To investigate if the lower number of TdTomato+ cells below the cortex in the mutant is caused by a disturbance in proliferation of the KDM5B KO cells, we analysed the relative number of alive TdTomato+ cells during FACS. We used this as a measure for the absolute number of TdTomato+ cells. Before FACS, DAPI is added to the dissociated cells from the isolated, electroporated cortex at E17. DAPI only marks dead cells. Therefore, it is possible to gate for live cells in the sample during FACS (Fig. 8A). From these live cells, we selected the TdTomato+ cells in both the KDM5B KO and GFP KO control (Fig. 8A). Looking at the percentage of TdTomato+ cells among the live cells showed that the relative number of TdTomato+ cells is significantly lower in the KDM5B KO (3,1 ± 1,01, p = 0,028) compared to the GFP KO control (5,98 ± 1,38) (Fig. 8B). Thus, this finding indicates that a loss of KDM5B results in a lower number of TdTomato+ cells compared to the control. Therefore, we propose that KDM5B is required for the proliferation of NSCs before they migrate towards the developing cortex.

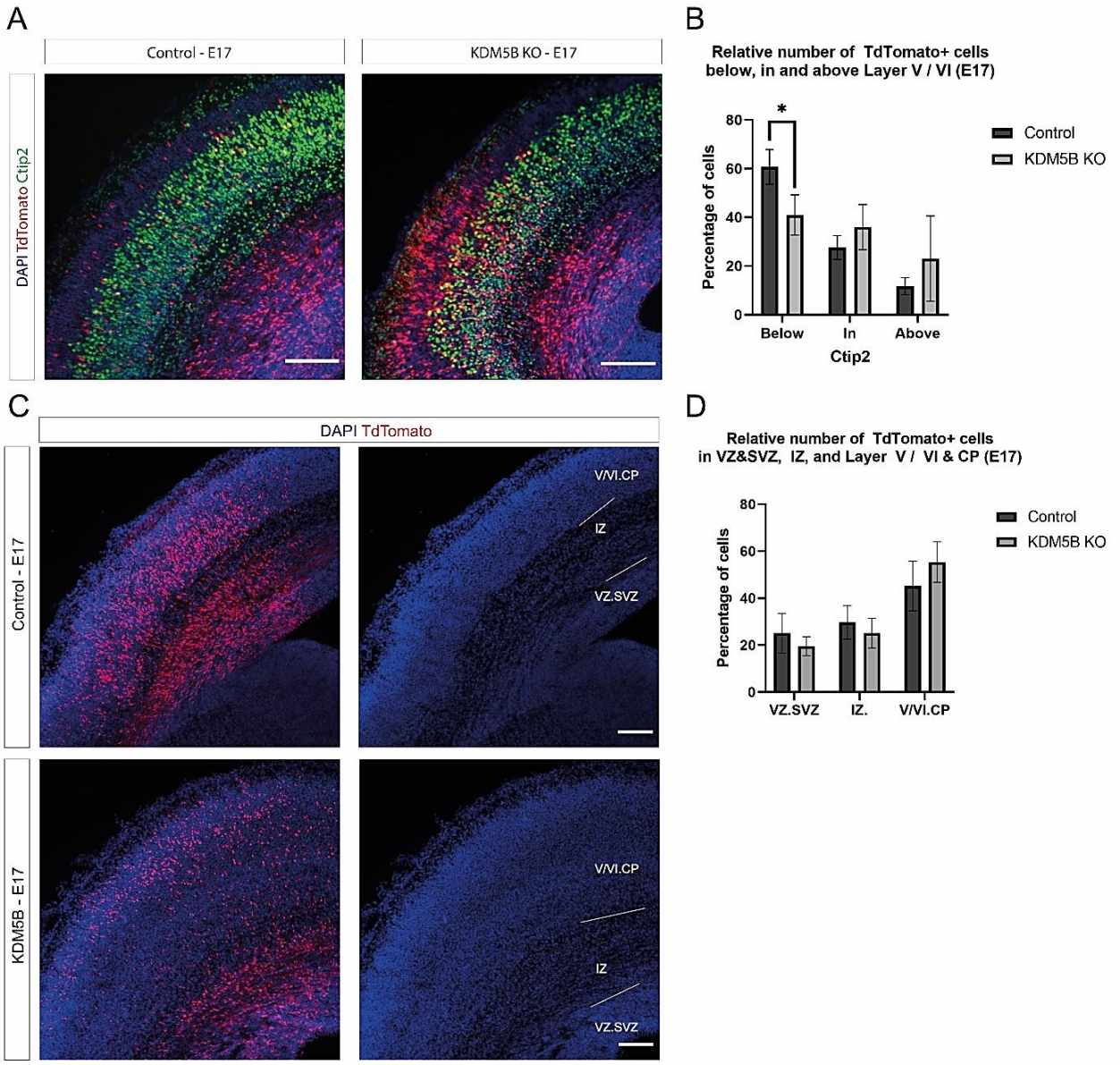

Figure 7 Effect of KDM5B KO on localization and migration of electroporated cells at E17.

(A) Exploration of the effect of KDM5B on the migration of TdTomato+ cells. Ctip2 indicates Layer V / VI (green). Scale bar = 500 µm.

*(B) Percentage of TdTomato+ cells below, in and below layer V / VI indicated by Ctip2. The relative number of TdTomato+ cells below layer V / VI is significantly lower in KDM5B KO compared to the GFP KO control. Statistics: Multiple student's T-test with Welch's correction; KDM5B KO, N = 3; GFP KO, N = 4, * = P < 0.05*

(C) Ventricular zone (VZ) and Subventricular zone (SVZ), intermediate zone (IZ) and layer V / VI and cortical plate (CP) in the electroporated cortex. Scale bar = 500 µm.

*(D) Percentage of TdTomato+ cells in VZ and SVZ, IZ or layer V / VI and CP. The relative amount of TdTomato+ cells in the VZ and SVZ, and IZ appears to be lower in the KDM5B KO compared to the GFP KO control. Statistics: Multiple student's T-test with Welch's correction; KDM5B KO, N = 4; GFP KO, N = 5, * = P < 0.05*

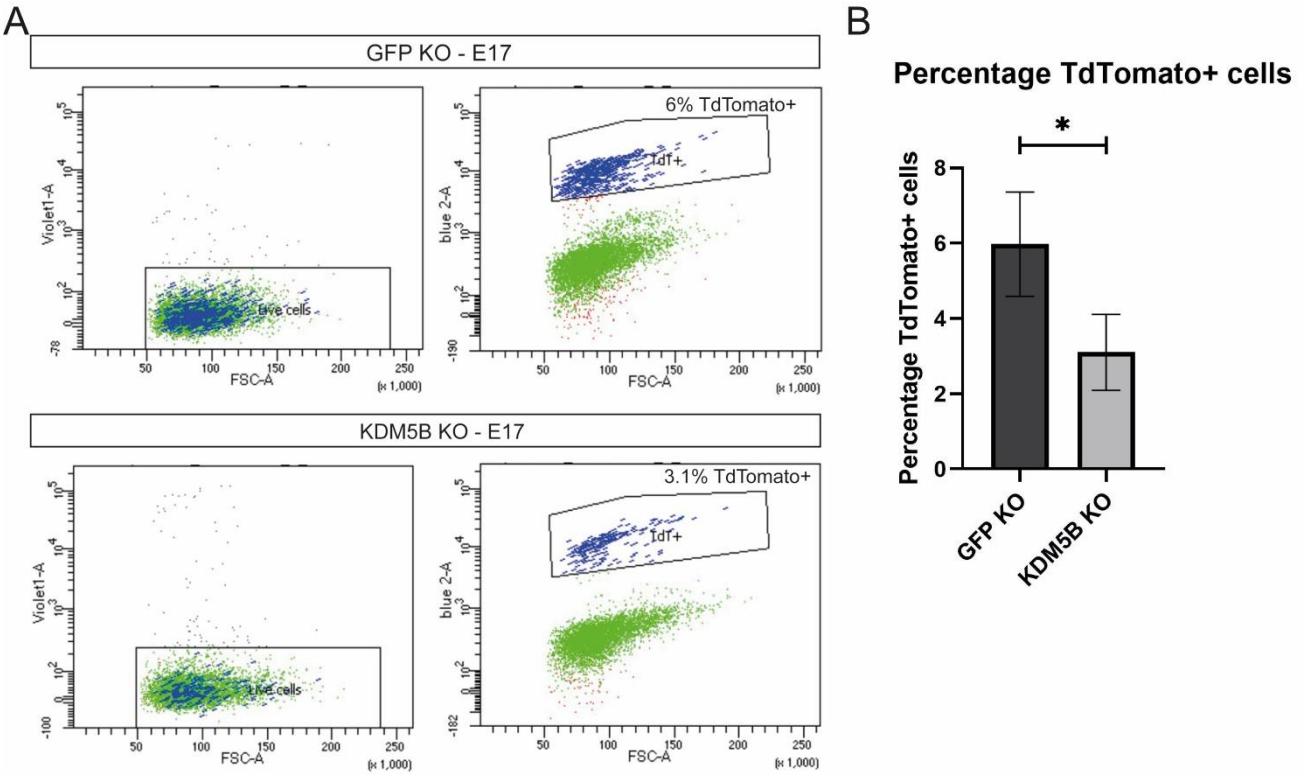

Figure 8 Relative number of TdTomato+ cells in KDM5B KO after FACS

(A) FACS analysis of GFP KO control and KDM5B KO at E17. 6% of the total number of live cells were TdTomato+ in the GFP KO. 3.1% of the live cells were TdTomato+ in KDM5B KO.

*(B) The percentage TdTomato+ cells among live cells is significantly lower in KDM5B KO compared to GFP KO control. Statistics: unpaired, parametric Welch's T-test; Mean ± SD; KDM5B KO, N = 4; GFP KO, N = 4; * = P < 0.05.*

In summary, the four gRNAs that we designed to target KDM5B are successfully cloned and inserted into a pCAG-Cre-U6-4xgRNA plasmid. IUE delivery of this plasmid leads to an effective CRISPR/Cas9-mediated gene inactivation of KDM5B. This results in a lower relative number of electroporated cells below layer V and VI in the mutant compared to the control at E17, which might be caused by a decreased proliferation of KDM5B KO cells.

Discussion

In this study, we study the effect of KDM5B on cortical development after creating a KDM5B KO by inactivating KDM5B using the CRISPR/Cas9 system. The CRISPR/Cas9 pipeline that is developed in the Basak lab utilizes four gRNAs that I have designed to target KDM5B. After cloning the four gRNAs, all the gRNAs are inserted in the same plasmid, which is introduced into embryos at E13 with an IUE. FACS analysis showed that CRISPR/Cas9 system is functional. As a result, we observed a lower expression of KDM5B in electroporated TdTomato+ cells in the mutant compared to the control, which is a first indication that a KDM5B KO has been generated with the CRISPR/Cas9 system. A KDM5B KO results in a relatively lower number of TdTomato+ cells below layers V and VI compared to the control. We observed

a relatively lower total number of KDM5B KO cells during FACS, which leads to our suggestion that this lower number is due to a disrupted proliferation of mutant cells. The observation that KDM5B is mostly expressed in the ventricular zone at E17 supports our conclusion that KDM5B is most likely indispensable for neurogenesis in the VZ and newborn neurons.

The observed lower relative number of TdTomato+ cells below layer V and VI in the mutant can have several causes. First, KDM5B KO cells may start migrating earlier. It has been observed that a KDM5B KO results in accelerated NSCs migration *in vitro* (Zhou et al., 2016). Furthermore, KDM5B serves as a repressor of genes involved in migration in triple-negative breast cancer cells (Han et al., 2017; Klein et al., 2014). A first look at the localization of TdTomato+ cells relative to layer V and VI in the mutant compared to the control would indeed suggest that the KDM5B KO results in an accelerated migration of cells. It needs to be noted that these results are based on relative numbers. Since there are variations in dissection of embryos and the number of electroporated cells varies between samples, it is hard to look at the absolute number of electroporated cells. The fact that it is a relative amount of TdTomato+ means that there are several other explanations for the observation that there are fewer KDM5B KO cells below layer V and VI compared to the control. NSCs below layer V and VI may die without KDM5B. Looking at the percentage of TdTomato+ cells among alive cells during FACS showed that there are fewer TdTomato+ cells in the KDM5B KO compared to the GFP KO control, which suggests that fewer electroporated cells survive without KDM5B. Depletion of KDM5B *in vitro* indeed decreases NSC and ESC proliferation (Dey et al., 2008; Zhou et al., 2016). KDM5B has been thought to maintain uncommitted precursors by repressing genes that regulate terminal differentiation (Dey et al., 2008). In contrast to this, other studies have shown KDM5B to be indispensable for initiating differentiation (Kidder et al., 2013; 2014; Schmitz et al., 2011). Dey *et al.* (2008) propose a commitment gradient in which cells downregulate KDM5B as they commit to a lineage and start differentiating and thereby losing their stem cell potential. Since we have shown that KDM5B is highly expressed in the VZ, we suggest that KDM5B is particularly important for neurogenesis in the VZ and newborn neurons. To assess if the KDM5B KO results in reduced proliferation of NSCs, a cell cycle assay with BrdU and Ki67 can be performed (Romar et al., 2016; Wojtowicz & Kee, 2006). With either a RT-qPCR or single-cell RNA sequencing (scRNAseq) it can be investigated if certain differentiation markers have a reduced or increased expression in the mutant to assess if and how the KDM5B KO has influenced the differentiation of NSCs. By doing so, we can confirm if KDM5B is indeed required for proliferation of NSCs or if KDM5B is involved in differentiation of NSCs as well.

Based on the decrease of KDM5B KO cells and the high expression of KDM5B in the VZ, we suggest that KDM5B is required for the proliferation of NSCs. Other studies have linked KDM5B to the proliferation of NSCs before (Cederquist et al., 2020; Dey et al., 2008). It is also suggested that KDM5B activates genes associated with the self-renewal of ESCs (Xie et al., 2011). KDM5B removes a methyl group from H3K4me3, which is part of bivalent chromatin modification with H3K27me3. Ezh2 that is part of PRC2 is responsible for methylation of H3K27. Ezh2 and PRC2 have been linked to the differentiation of NSCs (Corley & Kroll, 2015; Pereira et al., 2010; Zhang et al., 2014). Considering the commitment gradient suggested by Dey *et al. (2008),* KDM5B may be important during the proliferation of NSCs, while Ezh2 and PRC2 are more important during differentiation after this proliferation phase. To gain a better understanding of how the bivalent chromatin modification affects the development of the cortex, it would be interesting to combine a KDM5B KO with an Ezh2 KO in the future. Both the KDM5B and Ezh2 KO have been established in the Basak lab before. It showed us that an Ezh2 KO results in changes in migration in the postnatal brain, which was assessed at P7. No effects of the Ezh2 KO on migration at E17 have been observed in this study. If we look at the effect of a KDM5B / Ezh2 KO on proliferation, differentiation and migration at different timepoints during cortical development and compare this with the individual a KDM5B and Ezh2 KO, it will show us whether the absence of both histone modifiers results in different alterations in cortical development. This will give us a better understanding of the cooperation between KDM5B and PRC2 and how this influences cortical development.

Bivalent chromatin modification is likely dependent on the presence of both histone modifiers. Both KDM5B and Ezh2 / PRC2 are epigenetic regulators. With scRNAseq, we can look if a combined KDM5B / Ezh2 KO leads to a differential gene expression that has not been observed in an individual KDM5B or Ezh2 KO. An interesting addition to scRNAseq is to use chromatin immunoprecipitation followed by next-generation sequencing (ChIPseq), which is used to study the interaction between DNA and proteins. By using ChIPseq, we can establish if there are changes in binding sites of KDM5B on the DNA in the Ezh2 KO and the other way around and thus determine whether KDM5B requires Ezh2 to bind to certain genes.

It is important to consider that it is likely that KDM5B is not only involved in establishing bivalent chromatin modifications and thereby in repressing gene expression. Other studies have proposed that KDM5B is required for active gene transcription (Kurup et al., 2019; Xie et al., 2011). By localizing H3K4me4 to the transcriptional start site instead of the gene body, KDM5B ensures correct elongation of transcription (Xie et al., 2011). scRNAseq might therefore also show us a lower expression of particular genes when KDM5B is inactive.

Since KDM5B is an epigenetic regulator, the absence of functional KDM5B can lead to changes in gene expression. We can evaluate alterations in gene expression with scRNAseq. For this, we sorted TdTomato+ cells in 384-wells plates during FACS. Based on the fact that KDM5B is still expressed in 31% of the electroporated cells in the KDM5B KO, not all the sorted TdTomato+ cells are guaranteed to be a KDM5B KO. This makes it harder and less reliable to compare the mutant to the control during the analysis of the scRNAseq data to see if there is differential gene expression in the mutant. Further confirmation that we indeed successfully created multiple mutations in the KDM5B gene and thereby inactivated KDM5B is thus required before continuing with scRNAseq.

For the reliability of the results and the aforementioned decision to continue with scRNAseq, several aspects of the methodology should be discussed. Since earlier results showed that the established CRISPR/Cas9 and IUE pipeline was sufficient to generate a KO, we decided to immediately proceed with IUE gene delivery (Kalebic et al., 2016; Shinmyo et al., 2016). Especially after no mutations were found in the pCAG-Cre-U6-4xgRNA plasmid during Sanger sequencing. To get more reliable results with this CRISPR/Cas9 pipeline in the future, it might be beneficial to first test the plasmid *in vitro.* A possibility is to use microinjection into single neural stem cells in culture or transfection of NIH3T3 cells and assess whether the targeted gene is mutated and its expression is disrupted (Kalebic et al., 2016; Shinmyo et al., 2016). However, it should be noted that there is possibly difference in the functioning of the CRISPR/Cas9 system *in vivo* and *in vitro* (Shinmyo et al., 2016). In addition to this, it is important to consider possible off-target effects of the gRNAs before proceeding with IUE. Even though we considered off-target scores during the design of the gRNAs, the gRNAs can be tested to further confirm no off-target effects. For instance by looking at changes in the genome after *in vitro* Cas9 reactions (Kalebic et al., 2016).

It is important to also verify the KDM5B KO after the IUE. A possibility is to perform sequencing on the TdTomato+ cells that were isolated during FACS. Currently, a method for Sanger sequencing using primer pairs surrounding the target sites of the four gRNAs is being set up. Sanger sequencing is ideal to get the first indication of whether the four gRNAs have created a mutation in the Kdm5b gene. To get a more detailed picture of the mutations that have been created in the different electroporated cells, amplicon sequencing can be considered in the future. Another advantage of amplicon sequencing is that off-target effects can also be detected (Kalebic et al., 2016). In addition to this, we can use RT-qPCR of isolated TdTomato+ cells to see if targeting the TSS has led to a reduced expression of KDM5B. It should be kept in mind that TdTomato+ cells for DNA sequence and RNA expression analysis were only isolated after TdTomato+ cells were sorted into 384-wells plates for future

scRNAseq. The amount of material available is therefore limited, which can negatively impact the DNA sequence results.

Although we recommend further validation of the KDM5B KO, the different methods used in this study to verify the KDM5B KO still give a clear first indication that we have generated KDM5B KO. Immunohistochemistry with KDM5B showed that the functional CRISPR/Cas9 system reduced KDM5B expression in the KDM5B KO. It should be considered that the KDM5B staining on mutant and control did not always give quantifiable results. Furthermore, since KDM5B is part of the KDM5 family with a highly conserved domain architecture, it is possible that the KDM5B primary antibodies bind other members of the KDM5 family. Blasting the immunogen sequence showed that the KDM5B primary antibody can bind to KDM5A too. However, this would affect the control and the mutant equally. Together with the much lower alignment of the KDM5B primary antibody with KDM5A than with KDM5B, the observed difference in KDM5B expression between the mutant and control still reliably indicates a successful KDM5B KO.

To look at the KDM5B expression throughout the embryonic and postnatal development of the cortex, we performed RT-qPCR on isolated cortices and did an immunohistochemistry staining for KDM5B. Both methods show a relatively higher expression of KDM5B at late embryonic and early postnatal development timepoints. However, there were small differences in the observed expression levels between both methods. It should be noted that RT-qPCR measures mRNA levels in bulk, while immunohistochemistry visualizes proteins after their synthesis, which might explain the observed discrepancy. The lower relative expression at P7 and adult might also be explained by the fact that there are more cell types present. It is important to realize that RT-qPCR is performed in bulk, so other cell types such as astrocytes are also included in P7 and adult. This is not yet the case during early embryonic development timepoints. The observed decrease in relative expression at postnatal development might be due to these additional cell types, which would mean that the expression per cell is not decreasing.

By showing that KDM5B is important in proliferation of NSCs in the VZ, this study paves the first steps in gaining a better understanding of the role of KDM5B during cortical development. Linked to PRC2, our results will guide future studies focused on exploring bivalent chromatin modifications and their role in corticogenesis. The optimized CRISPR/Cas9 gene inactivation pipeline might be useful in these future studies. Unravelling how bivalent chromatin modifications affect cortical development will aid future studies addressing whether and how this epigenetic regulation is changed in ASD patients. After establishing the role of epigenetic

regulation in cortical development, it will be interesting to look into other high confidence ASD-linked genes. If more epigenetic regulators are implicated in ASD, future studies into therapeutic targets should consider changes in gene expression if their epigenetic regulators are mutated.

Methods

Mice

C57BL/6J mice were used for immunohistochemistry and RT-qPCR to look at KDM5B expression levels. *In utero* electroporation was performed in heterozygous offspring from crossing over Gt(ROSA)26Sortm14(CAG-tdTomato)Hze (LSL-TdTomato) mice with (ROSA)26Sortm1.1(CAG-cas9*,-EGFP)Fezh mice (Rosa-Cas9-GFP). All animal experiments were performed at the UMC Utrecht Brain Center, according to the regulations of the European Union (directive 2010/63/EU) and in consultation with the Animal Welfare Body (Instantie voor Dierenwelzijn) Utrecht. All specific pathogen-free animals are housed in a barrier facility, in which all personnel must wear protective clothing (caps and special clogs).

Designing gRNAs

CRISPR/Cas9 target sites in the genomic sequence of *Kdm5b* were identified. Four gRNAs targeting the transcriptional start site and 3 functional domains were selected based on on- and off-target scores and the presence of a PAM sequence with a CRISPR gRNA design tool (https://www.benchling.com/crispr/) (Sequences and on- and off-targets scores are provided in Table I).

Table I: 4 gRNAs designed to target Kdm5b

Name	Position	Sequence	PAM	On-target	Off-target	Domain
Kdm5b_TSS_FW1	134560184	TAGCGGCAAGACGTCGTCGG	AGG	65.3	98.8	TSS
Kdm5b_ex2_RV2	134585169	TCGACATCACAAGCGAATGG	TGG	69.2	90.1	JmjN
Kdm5b_ex8_RV3	134599176	AGTCTCCCTTGGGAACGTCA	TGG	61.6	79.0	PHD1
Kdm5b_ex27_FW4	134631645	GGGGTCTCTACTGATTACGA	AGG	74.1	94.4	PHD3

Amplification oligo gRNAs

The oligo gRNAs were purchased from Integrated DNA Technologies (sequences provided in Table II). The gRNAs in oligo pairs were phosphorylated and annealed with T4 polynucleotide Kinase in 10x T4 Ligase buffer (ThermoFischer Scientific) using a thermocycler with the following parameters: 37°C – 30'; 95°C – 5', ramp down to 25°C at 5°C/min; 12°C – ∞. The annealed oligo gRNAs were diluted 1 : 200 into sterile water. T4 ligase in 10x T4 ligase buffer was used in the ligation reaction of the diluted oligo duplexes and previously BbsI-digested

(NEB) pCAG-Cre-U6 plasmids. The ligation reaction was set up at RT for 20 minutes and put on ice afterwards.

Table II sgRNAs in oligo pairs

Name	Sequence
gRNA_Kdm5b_TSS_FWD1	CACCGTAGCGGCAAGACGTCGTCGG
gRNA_Kdm5b_TSS_RV1	AAACCCGACGACGTCTTGCCGCTAC
gRNA_Kdm5b_ex2_FW2	CACCGCCATTCGCTTGTGATGTCGA
gRNA_Kdm5b_ex2_RV2	AAACTCGACATCACAAGCGAATGGC
gRNA_Kdm5b_ex8_FW3	CACCGTGACGTTCCCAAGGGAGACT
gRNA_Kdm5b_ex8_RV3	AAACAGTCTCCCTTGGGAACGTCAC
gRNA_Kdm5b_ex27_FW4	CACCGGGGGTCTCTACTGATTACGA
gRNA_Kdm5b_ex27_RV4	AAACTCGTAATCAGTAGAGACCCCC

The red sequence is added to anneal with the overhang of the digested plasmid.

Transformation

Competent Dh5α bacteria were used for transformation. 5 µl of the ligation reaction was mixed with 50 µl of the competent cells and incubated on ice for 30' and then transferred to 37°C for 5' as heat-shock. The heat-shocked cells were returned to ice for 2'. The competent cells were incubated with prewarmed 1x Luria-Bertani broth (LB) (FisherScientific) for 37°C for 30' for recovery. After spinning down the bacteria at 6000 rpm for 30s, the transformed bacteria are transferred onto 1x LB plates with ampicillin (Sigma, #A9518-25g) (100mg / µl) and grown overnight.

After picking colonies and growing them overnight in LB with ampicillin (100mg / µl), the plasmids were purified from the competent cells using miniprep plasmid isolation (QIAprep spin column kit). The purified plasmids were sent for Sanger sequencing to verify the gRNA cassette sequence (Sequencing Primers in Table III).

Table III Sequencing Primers

Name	Function	Sequence
pCAG-cre-U6 4301-4324_FW	Sequence from U6 promoter to 3' into the 1xgRNA	ACGATACAAGGCTGTTAGAGAGAT
pCAG-cre-U6 4665-4686_RV	Sequence into 1xgRNA scaffold from the 3'	ATTTGTCTGCAGAATTGGCGCA
pCre-U6-gRNA_ori_FW	Sequence from U6 promoter to 3' into the 4xgRNA	AGGTATCCGGTAAGCGGCAGGG
pCre-U6-gRNA_cmv_RV	Sequence into 4xgRNA scaffold from the 3'	TATTGACGTCAATGGGCGGGGG

Gibson Assembly 4xgRNAs

Three of the four purified single constructs were amplified with KOD polymerase PCR (Millipore), according to the manufacturer's protocol. Primer sequences are provided in Table IV. The construct containing the fourth gRNA cassette was digested with HindIII (Roche Diagnostics, 10 U/µl) at 37°C for 3h. The pCAG-Cre-U6-gRNA construct with a single cut served as the backbone for Gibson assembly. Both the single-cut plasmid and gRNA cassettes were run on a 1% and 2% agarose gel respectively. DNA was purified from the gel with Purelink Gel extraction kit. To generate the 4xgRNA construct, the three sgRNA cassettes and single-cut sgRNA plasmid were incubated with Assembly Master Mix (NEB) in a thermocycler at 50°C for 1h. The pCAG-Cre-U6-4xgRNA constructs were transformed into competent cells as described before and grown overnight. After extracting the plasmids from the competent cells with miniprep plasmid isolation (Qiagen), the insertion of the four gRNA cassettes was confirmed by the correct size after performing a gel restriction digestion (XbaI and XhoI or SalI, Roche Diagnostics, 10 U/µl) and Sanger sequencing (primers provided in Table III). The final pCAG-Cre-U6-4xgRNA construct was amplified by an overnight culture and purified using a maxiprep (Qiagen), as described before.

Table IV Primers PCR amplification for Gibson Assembly

Name	Sequence
pCAG-Cre-U6_4x_fw1	GACAAATGGCTCTAGAAGCT**GAGGGCCTATTTCCCATGATTC**
pCAG-Cre-U6_4x_rv1	GGTTGGGAGGTGGGTCTGAA**AAAACAAAAAAGCACCGACT**
pCAG-Cre-U6_4x_fw2	TTCAGACCCACCTCCCAACC**GAGGGCCTATTTCCCATGATTC**
pCAG-Cre-U6_4x_rv2	TTCACTAATCGAATGGATCT**AAAACAAAAAAGCACCGACT**
pCAG-Cre-U6_4x_fw3	AGATCCATTCGATTAGTGAA**GAGGGCCTATTTCCCATGATTC**
pCAG-Cre-U6_4x_fw3	TCGACAATTGCTAGCAAGCT**AAAACAAAAAAGCACCGACT**

The red sequence is added to the pCAG-Cre-U6-gRNA sequence to create complementarity during Gibson Assembly.

In Utero Electroporation

In utero electroporation was performed by trained technicians with my assistance in pregnant mice at E13. Mice were intraperitoneally injected with buprenorphine (0.1 ml g^{-1}) 30 minutes prior to surgery. Mice were then anaesthetized with isoflurane (induction: 5%; surgery: 1.5 – 2%). The peritoneal cavity was surgically opened and the uterus with embryos was taken out of the abdominal cavity. The embryos were injected with 1 µl pCAG-Cre-U6-4xgRNA construct (1 µg / µl) with Fast Green Cycle dye (10% of total volume) (Sigma-Aldrich) into the lateral

ventricles with a pulled glass needle. The embryo's head was held between two circular electrodes and a third electrode was placed between them (Fig. 9). Five pulses (30V, 50ms duration, 950ms interval) were delivered for electroporation. The embryos were carefully returned into the abdominal cavity and allowed to continue to develop until isolation at E17.

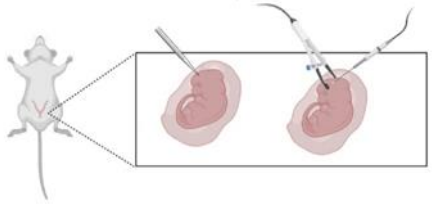

Figure 9 Overview of in utero electroporation. *The pCAG-Cre-U6-4xgRNA construct in a fluid with Fast Green Cycle dye is injected into the ventricles with a pulled glass needle. Three electrodes are placed around the head region to introduce the construct into NSCs with a negative charge.*

RNA isolation, cDNA synthesis and RT-qPCR

Cortices from C57BL/6J embryos and mice were collected at E10, E13, E17, E18, P4, P7 and adult (N = 3). The tissue was frozen and stored at -80 until RNA isolation. RNA was isolated with the RNeasy Mini Kit (Qiagen) following the supplied protocol. cDNA was synthesized from the isolated RNA with the SuperScript IV Reverse Transcriptase kit (Invitrogen) and oligo d(T)20 primers (Invitrogen). The generated cDNA was diluted 1 : 10 before proceeding with the RT-qPCR.

2x Sybr Green (Qiagen) was mixed with primer pairs and water before adding cDNA. Primer sequences of the primers used are provided in Table V. A standard curve with combined cDNA was made with 1:3, 1:10, 1:30 and 1:100 dilutions of undiluted cDNA generated from P7 isolated cortices. GAPDH and β-actin were used as housekeeping genes to normalize during the analysis of the data. Expression levels were analysed by calculating the relative fold gene expression level ($2^{-\Delta\Delta Ct}$) with the cycle threshold (Ct).

Table V Primers for qPCR

Name	Sequence
qPCR_Kdm5b_1_FW	ACAGAGTTGTCTCCCCCTCC
qPCR_Kdm5b_1_RV	CGAAGGCAATCGTTCTTCTCAC
qPCR_Kdm5b_3_FW	ACAGAGTTGTCTCCCCCTCCA
qPCR_Kdm5b_3_RV	CCTCGAAGGCAATCGTTCTTCTC
qPCR_GAPDH_FW	TCCATGACAACTTTGGCATCGTGG
qPCR_GAPDH_RV	GTTGCTGTTGAAGTCACAGCAGAC
qPCR_βActin_FW	GATGACGATATCGCTGCGCTG
qPCR_βActin_RV	GCCTGTGGTACGACCAGAGGC

Immunohistochemistry

Embryonic brains were collected at E10, E13, E14, E17 and E18 after cervical dislocation of the mother. Postnatal brains from electroporated embryos were obtained at P7 after perfusion of the pups. Non-electroporated brains were isolated from WT mice at P4 and P7 without perfusion. The isolated brains were fixed in 4% paraformaldehyde in 1xPBS on a shaker at 4 °C overnight. After washing the fixed brains, the brains were cryoprotected by 30% sucrose (Merck Millipore) before freezing and storing them at -80 °C. 20-25 µm thick sections were cut on a cryostat and placed on SuperFrost Plus glass slides (VWR).

Antigen Retrieval: For the use of KDM5B, H3K4me3 and Ctip2 primary antibodies, antigen retrieval was performed. A 3% tri-sodium citrate dihydrate (Merck Millipore) solution was made in autoclaved water. The pH was adjusted to 6.0 with 1N HCl. After rehydrating the slides with PBS for 5', the slides were placed in the tri-sodium citrate dihydrate buffer and placed in the microwave at 180W for 7'. The slides were cooled down in the buffer solution for 30' before proceeding with a washing step and the normal immunohistochemistry protocol.

Staining: After rehydration with PBS, slides were blocked with 5% normal donkey serum in 0.05% TritonX-100 PBS for 30'. The sections were incubated with primary antibodies at 4 °C o/n, washed 3 x 5' with 1xPBS and incubated with the complementary secondary antibodies at RT for 2 hours. DAPI (1:2000 from 4mg/ml stock) was added to the sections for 10' before washing them 3 x 5' with 1xPBS. The sections were mounted in Fluorsave Mounting Medium Reagent (Calbiochem).

Antibodies: Primary antibodies: Rabbit anti-KDM5B (SigmaAldrich, HPA053723), conc: 1 : 1000; Rabbit anti-H3K4me3 (Thermofisher), conc: 1 : 200; Rat anti-Ctip2 (Abcam, # ab18465), conc: 1 : 500. Secondary antibodies: AF488 – donkey-anti-rabbit (ThermoFisher, #A21206); AF647 – donkey-anti-rabbit (LifeTechnologies, #A-31573), conc: 1:1000; AF647 – donkey-anti-rat (Abcam, # ab150155); conc: 1:1000.

Analysis: Microscopic pictures were taken with a epi-fluorescence microscope (Zeiss Axio Scope A1) or confocal microscope (Olympus FV1000). Images were processed similarly in Fiji (ImageJ) before localization and colocalization were determined manually with CellCounter. A trial was done for automated counting using the "Analyse Particles" plugin of Fiji (ImageJ). This gave inconsistent results, so the analysis was done manually.

Flow Cytometry / FACS

Brains were collected at E17 in DMEM/F-12 (Thermofisher), and the fluorescent electroporated area was isolated under a fluorescent microscope. The targeted area was incubated with papain (Worthington) at 37°C for 15'. Afterwards, DNase I (Neural Tissue Dissection Kit, MACS / Worthington) was added. After mechanically dissociating the tissue by pipetting up and down, the tissue was incubated again at 37°C for 15'. Pressure was applied during the second mechanical dissociation step. The dissociated tissue was washed by adding 2% FBS (ThermoFisher) in DMEM/F-12 and spinning it down 1000 rpm for 7'. After discarding the supernatant, the wash step was repeated. The cells were resuspended in DMEM/F-12 containing ROCK inhibitor (1:2000, MedChemExpress) and filtered through a 40 µm mesh nylon filter (Corning) into a sterile FACS tube (FALCON). DAPI (1 : 1000, 1 µg/ml) was added shortly before the FACS sorting. Single TdTomato+ cells were sorted onto 384-wells plates, which were frozen on dry ice before being placed at -80°C. The remaining TdTomato+ cells were sorted into tubes for DNA sequencing and RNA sequencing. Tubes were stored at -20 after spinning them down with 1500 rpm (~200xg [rcf]) for 5' and removing as much supernatant as possible. For RNA sequencing, RTL lysis buffer (RNeasy Mini Kit, Qiagen) was added.

References

Adli, M. (2018). The CRISPR tool kit for genome editing and beyond. *Nature Communications, 9*(1), 1-13.

Albert, M., & Huttner, W. B. (2018). Epigenetic and transcriptional pre-patterning—An emerging theme in cortical neurogenesis. *Frontiers in Neuroscience, 12*, 359.

Albert, M., Kalebic, N., Florio, M., Lakshmanaperumal, N., Haffner, C., Brandl, H., . . . Huttner, W. B. (2017). Epigenome profiling and editing of neocortical progenitor cells during development. *The EMBO Journal, 36*(17), 2642-2658.

Albert, M., Schmitz, S. U., Kooistra, S. M., Malatesta, M., Torres, C. M., Rekling, J. C., . . . Helin, K. (2013). The histone demethylase Jarid1b ensures faithful mouse development by protecting developmental genes from aberrant H3K4me3. *PLoS Genet, 9*(4), e1003461.

Barski, A., Cuddapah, S., Cui, K., Roh, T., Schones, D. E., Wang, Z., . . . Zhao, K. (2007). High-resolution profiling of histone methylations in the human genome. *Cell, 129*(4), 823-837.

Baxter, A. J., Brugha, T. S., Erskine, H. E., Scheurer, R. W., Vos, T., & Scott, J. G. (2015). The epidemiology and global burden of autism spectrum disorders. *Psychological Medicine, 45*(3), 601-613.

Bernstein, B. E., Mikkelsen, T. S., Xie, X., Kamal, M., Huebert, D. J., Cuff, J., . . . Plath, K. (2006). A bivalent chromatin structure marks key developmental genes in embryonic stem cells. *Cell, 125*(2), 315-326.

Cederquist, G. Y., Tchieu, J., Callahan, S. J., Ramnarine, K., Ryan, S., Zhang, C., . . . Zhou, T. (2020). A multiplex human pluripotent stem cell platform defines molecular and functional subclasses of autism-related genes. *Cell Stem Cell, 27*(1), 35-49. e6.

Chen, R., Davis, L. K., Guter, S., Wei, Q., Jacob, S., Potter, M. H., . . . Li, B. (2017). Leveraging blood serotonin as an endophenotype to identify de novo and rare variants involved in autism. *Molecular Autism, 8*(1), 1-12.

Corley, M., & Kroll, K. L. (2015). The roles and regulation of polycomb complexes in neural development. *Cell and Tissue Research, 359*(1), 65-85.

Courchesne, E., Pierce, K., Schumann, C. M., Redcay, E., Buckwalter, J. A., Kennedy, D. P., & Morgan, J. (2007). Mapping early brain development in autism. *Neuron, 56*(2), 399-413.

De Dieuleveult, M., Yen, K., Hmitou, I., Depaux, A., Boussouar, F., Dargham, D. B., . . . Baulard, C. (2016). Genome-wide nucleosome specificity and function of chromatin remodellers in ES cells. *Nature, 530*(7588), 113-116.

De Rubeis, S., He, X., Goldberg, A. P., Poultney, C. S., Samocha, K., Cicek, A. E., . . . Walker, S. (2014). Synaptic, transcriptional and chromatin genes disrupted in autism. *Nature, 515*(7526), 209-215.

Dey, B. K., Stalker, L., Schnerch, A., Bhatia, M., Taylor-Papidimitriou, J., & Wynder, C. (2008). The histone demethylase KDM5b/JARID1b plays a role in cell fate decisions by blocking terminal differentiation. *Molecular and Cellular Biology, 28*(17), 5312-5327.

Doudna, J. A., & Charpentier, E. (2014). The new frontier of genome engineering with CRISPR-Cas9. *Science, 346*(6213)

Garcia-Forn, M., Boitnott, A., Akpinar, Z., & De Rubeis, S. (2020). Linking autism risk genes to disruption of cortical development. *Cells, 9*(11), 2500.

Gaugler, T., Klei, L., Sanders, S. J., Bodea, C. A., Goldberg, A. P., Lee, A. B., . . . Reichert, J. (2014). Most genetic risk for autism resides with common variation. *Nature Genetics, 46*(8), 881-885.

Genescu, I., & Garel, S. (2021). Being superficial: A developmental viewpoint on cortical layer 1 wiring. *Current Opinion in Neurobiology, 66*, 125-134.

Gesuita, L., & Karayannis, T. (2021). A 'Marginal'tale: The development of the neocortical layer 1. *Current Opinion in Neurobiology, 66*, 37-47.

Gilbert, S. J., Bird, G., Brindley, R., Frith, C. D., & Burgess, P. W. (2008). Atypical recruitment of medial prefrontal cortex in autism spectrum disorders: An fMRI study of two executive function tasks. *Neuropsychologia, 46*(9), 2281-2291.

Götz, M., & Huttner, W. B. (2005). The cell biology of neurogenesis. *Nature Reviews Molecular Cell Biology, 6*(10), 777-788.

Grove, J., Ripke, S., Als, T. D., Mattheisen, M., Walters, R. K., Won, H., . . . Anney, R. (2019). Identification of common genetic risk variants for autism spectrum disorder. *Nature Genetics, 51*(3), 431-444.

Han, M., Xu, W., Cheng, P., Jin, H., & Wang, X. (2017). Histone demethylase lysine demethylase 5B in development and cancer. *Oncotarget, 8*(5), 8980.

Harikumar, A., & Meshorer, E. (2015). Chromatin remodeling and bivalent histone modifications in embryonic stem cells. *EMBO Reports, 16*(12), 1609-1619.

Hsu, P. D., Lander, E. S., & Zhang, F. (2014). Development and applications of CRISPR-Cas9 for genome engineering. *Cell, 157*(6), 1262-1278.

Kalebic, N., Taverna, E., Tavano, S., Wong, F. K., Suchold, D., Winkler, S., . . . Sarov, M. (2016). CRISPR/Cas9-induced disruption of gene expression in mouse embryonic brain and single neural stem cells in vivo. *EMBO Reports, 17*(3), 338-348.

Kidder, B. L., Hu, G., Yu, Z., Liu, C., & Zhao, K. (2013). Extended self-renewal and accelerated reprogramming in the absence of Kdm5b. *Molecular and Cellular Biology, 33*(24), 4793-4810.

Kidder, B. L., Hu, G., & Zhao, K. (2014). KDM5B focuses H3K4 methylation near promoters and enhancers during embryonic stem cell self-renewal and differentiation. *Genome Biology, 15*(2), 1-19.

Klein, B. J., Piao, L., Xi, Y., Rincon-Arano, H., Rothbart, S. B., Peng, D., . . . Zheng, X. (2014). The histone-H3K4-specific demethylase KDM5B binds to its substrate and product through distinct PHD fingers. *Cell Reports, 6*(2), 325-335.

Kurup, J. T., Campeanu, I. J., & Kidder, B. L. (2019). Contribution of H3K4 demethylase KDM5B to nucleosome organization in embryonic stem cells revealed by micrococcal nuclease sequencing. *Epigenetics & Chromatin, 12*(1), 1-18.

Lauberth, S. M., Nakayama, T., Wu, X., Ferris, A. L., Tang, Z., Hughes, S. H., & Roeder, R. G. (2013). H3K4me3 interactions with TAF3 regulate preinitiation complex assembly and selective gene activation. *Cell, 152*(5), 1021-1036.

Li, J., You, Y., Yue, W., Yu, H., Lu, T., Wu, Z., . . . Zhang, D. (2016). Chromatin remodeling gene EZH2 involved in the genetic etiology of autism in chinese han population. *Neuroscience Letters, 610*, 182-186.

Lodato, S., & Arlotta, P. (2015). Generating neuronal diversity in the mammalian cerebral cortex. *Annual Review of Cell and Developmental Biology, 31*, 699-720.

Lord, C., Brugha, T. S., Charman, T., Cusack, J., Dumas, G., Frazier, T., . . . State, M. W. (2020). Autism spectrum disorder. *Nature Reviews Disease Primers, 6*(1), 1-23.

Lui, J. H., Hansen, D. V., & Kriegstein, A. R. (2011). Development and evolution of the human neocortex. *Cell, 146*(1), 18-36.

Maenner, M. J., Shaw, K. A., & Baio, J. (2020). Prevalence of autism spectrum disorder among children aged 8 years—autism and developmental disabilities monitoring network, 11 sites, united states, 2016. *MMWR Surveillance Summaries, 69*(4), 1.

Masini, E., Loi, E., Vega-Benedetti, A. F., Carta, M., Doneddu, G., Fadda, R., & Zavattari, P. (2020). An overview of the main genetic, epigenetic and environmental factors involved in autism spectrum disorder focusing on synaptic activity. *International Journal of Molecular Sciences, 21*(21), 8290.

Mosammaparast, N., & Shi, Y. (2010). Reversal of histone methylation: Biochemical and molecular mechanisms of histone demethylases. *Annual Review of Biochemistry, 79*, 155-179.

Mukhtar, T., & Taylor, V. (2018). Untangling cortical complexity during development. *Journal of Experimental Neuroscience, 12*, 1179069518759332.

Pereira, J. D., Sansom, S. N., Smith, J., Dobenecker, M., Tarakhovsky, A., & Livesey, F. J. (2010). Ezh2, the histone methyltransferase of PRC2, regulates the balance between self-renewal and differentiation in the cerebral cortex. *Proceedings of the National Academy of Sciences, 107*(36), 15957-15962.

Pokholok, D. K., Harbison, C. T., Levine, S., Cole, M., Hannett, N. M., Lee, T. I., . . . Herbolsheimer, E. (2005). Genome-wide map of nucleosome acetylation and methylation in yeast. *Cell, 122*(4), 517-527.

Romar, G. A., Kupper, T. S., & Divito, S. J. (2016). Research techniques made simple: Techniques to assess cell proliferation. *Journal of Investigative Dermatology, 136*(1), e1-e7.

Ronan, J. L., Wu, W., & Crabtree, G. R. (2013). From neural development to cognition: Unexpected roles for chromatin. *Nature Reviews Genetics, 14*(5), 347-359.

Salinas, R. D., Connolly, D. R., & Song, H. (2020). Invited review: Epigenetics in neurodevelopment. *Neuropathology and Applied Neurobiology, 46*(1), 6-27.

Sanders, S. J., He, X., Willsey, A. J., Ercan-Sencicek, A. G., Samocha, K. E., Cicek, A. E., . . . Dong, S. (2015). Insights into autism spectrum disorder genomic architecture and biology from 71 risk loci. *Neuron, 87*(6), 1215-1233.

Satterstrom, F. K., Kosmicki, J. A., Wang, J., Breen, M. S., De Rubeis, S., An, J., . . . Klei, L. (2020). Large-scale exome sequencing study implicates both developmental and functional changes in the neurobiology of autism. *Cell, 180*(3), 568-584. e23.

Schmitz, S. U., Albert, M., Malatesta, M., Morey, L., Johansen, J. V., Bak, M., . . . Helin, K. (2011). Jarid1b targets genes regulating development and is involved in neural differentiation. *The EMBO Journal, 30*(22), 4586-4600.

Shinmyo, Y., Tanaka, S., Tsunoda, S., Hosomichi, K., Tajima, A., & Kawasaki, H. (2016). CRISPR/Cas9-mediated gene knockout in the mouse brain using in utero electroporation. *Scientific Reports, 6*(1), 1-13.

Stiles, J., & Jernigan, T. L. (2010). The basics of brain development. *Neuropsychology Review, 20*(4), 327-348.

Straub, C., Granger, A. J., Saulnier, J. L., & Sabatini, B. L. (2014). CRISPR/Cas9-mediated gene knock-down in post-mitotic neurons. *PloS One, 9*(8), e105584.

Tick, B., Bolton, P., Happé, F., Rutter, M., & Rijsdijk, F. (2016). Heritability of autism spectrum disorders: A meta-analysis of twin studies. *Journal of Child Psychology and Psychiatry, 57*(5), 585-595.

Van Ingen, H., van Schaik, F. M., Wienk, H., Ballering, J., Rehmann, H., Dechesne, A. C., . . . Boelens, R. (2008). Structural insight into the recognition of the H3K4me3 mark by the TFIID subunit TAF3. *Structure, 16*(8), 1245-1256.

Vermeulen, M., Mulder, K. W., Denissov, S., Pijnappel, W. P., van Schaik, F. M., Varier, R. A., . . . Timmers, H. T. M. (2007). Selective anchoring of TFIID to nucleosomes by trimethylation of histone H3 lysine 4. *Cell, 131*(1), 58-69.

Vos, T., Allen, C., Arora, M., Barber, R. M., Bhutta, Z. A., Brown, A., . . . Chen, A. Z. (2016). Global, regional, and national incidence, prevalence, and years lived with disability for 310 diseases and injuries, 1990–2015: A systematic analysis for the global burden of disease study 2015. *The Lancet, 388*(10053), 1545-1602.

Wojtowicz, J. M., & Kee, N. (2006). BrdU assay for neurogenesis in rodents. *Nature Protocols, 1*(3), 1399-1405.

Woodworth, M. B., Greig, L. C., Kriegstein, A. R., & Macklis, J. D. (2012). SnapShot: Cortical development. *Cell, 151*(4), 918-918. e1.

Xhabija, B., & Kidder, B. L. (2019). (2019). KDM5B is a master regulator of the H3K4-methylome in stem cells, development and cancer. Paper presented at the *Seminars in Cancer Biology, , 57* 79-85.

Xie, L., Pelz, C., Wang, W., Bashar, A., Varlamova, O., Shadle, S., & Impey, S. (2011). KDM5B regulates embryonic stem cell self-renewal and represses cryptic intragenic transcription. *The EMBO Journal, 30*(8), 1473-1484.

Yao, B., Christian, K. M., He, C., Jin, P., Ming, G., & Song, H. (2016). Epigenetic mechanisms in neurogenesis. *Nature Reviews Neuroscience, 17*(9), 537.

Yao, B., & Jin, P. (2014). Unlocking epigenetic codes in neurogenesis. *Genes & Development, 28*(12), 1253-1271.

Yoon, S. H., Choi, J., Lee, W. J., & Do, J. T. (2020). Genetic and epigenetic etiology underlying autism spectrum disorder. *Journal of Clinical Medicine, 9*(4), 966.

Zhang, Y., Liang, J., & Li, Q. (2014). Coordinated regulation of retinoic acid signaling pathway by KDM5B and polycomb repressive complex 2. *Journal of Cellular Biochemistry, 115*(9), 1528-1538.

Zhou, Q., Obana, E. A., Radomski, K. L., Sukumar, G., Wynder, C., Dalgard, C. L., & Doughty, M. L. (2016). Inhibition of the histone demethylase Kdm5b promotes neurogenesis and derepresses reln (reelin) in neural stem cells from the adult subventricular zone of mice. *Molecular Biology of the Cell, 27*(4), 627-639.